Journal of Sol-Gel Science and Technology (2019) 90:359–368
https://doi.org/10.1007/s10971-019-04947-y

ORIGINAL PAPER: NANO-STRUCTURED MATERIALS (PARTICLES, FIBERS, COLLOIDS, COMPOSITES, ETC.)

The effects of precipitants on co-precipitation synthesis of yttria-stabilized zirconia nanocrystalline powders

Zhangyi Huang[1] · Wei Han[1,2] · Zhao Feng[1,3] · Jianqi Qi[1,3] · Di Wu[4] · Nian Wei[1,2] · Zhe Tang[1,2] · Yutong Zhang[1] · Junjing Duan[1] · Tiecheng Lu[1,2,3]

Received: 4 July 2018 / Accepted: 21 February 2019 / Published online: 28 February 2019

Abstract

Yttrium-stabilized zirconia ($Y_{0.08}Zr_{0.92}O_{1.96}$, YSZ) nanocrystalline powders were prepared by co-precipitation methods. Different precipitants (ammonium hydroxide, ammonium bicarbonate, oxalic acid, and urea) were used to study the effects of precipitants on co-precipitation synthesis of YSZ nanocrystalline powders. Thermogravimetric analysis-differential scanning calorimetry, powder X-ray diffraction, Fourier-transform infrared, scanning electron microscope, energy-dispersive spectrometer, Brunauer–Emmett–Teller, Barrett–Joyner–Halenda, and X-ray photoelectron spectroscopy analysis methods were employed to investigate the thermal decompositions, phase evolutions, micro-morphologies, surface areas, and elements analysis of the synthesized YSZ precursor powders or nanoparticles. Although different precipitants were used, the calcined products at 600 °C have nearly identical chemical compositions. The crystallization temperature of the precursor powders to evolve to cubic phase is the lowest (about 400 °C) when ammonium hydroxide is used as a precipitant, while it is about 500 °C in the case of other three types of precipitants (ammonium bicarbonate, oxalic acid, and urea) that were used. Ammonium bicarbonate cannot precipitate ZrO^{2+} effectively in the solution, resulting in the formation of cubic $Y_{0.18}Zr_{0.82}O_{1.91}$ at 1000 °C. Despite the time-consuming co-precipitation process, urea was proved to be the optimal precipitant in terms of the fabrication of nanocrystalline YSZ powders with designed Y/Zr/O molar ratio, large surface area, small crystallite size, and well dispersion.

Graphical Abstract

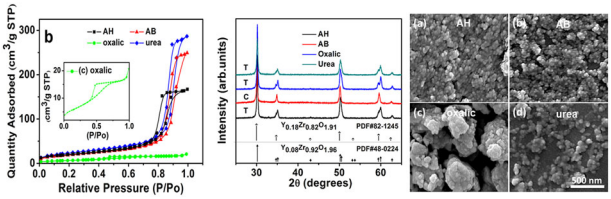

✉ Jianqi Qi
qijianqi@scu.edu.cn

✉ Tiecheng Lu
lutiecheng@scu.edu.cn

[1] College of Physical Science and Technology, Sichuan University, 610064 Chengdu, People's Republic of China

[2] Key Laboratory of High Energy Density Physics of Ministry of Education, Sichuan University, 610064 Chengdu, Sichuan, People's Republic of China

[3] Key Laboratory of Radiation Physics and Technology of Ministry of Education, Sichuan University, 610064 Chengdu, Sichuan, People's Republic of China

[4] The Gene and Linda Voiland School of Chemical Engineering and Bioengineering and the Alexandra Navrotsky Institute for Experimental Thermodynamics, Washington State University, Pullman, WA 99164, USA

Highlights

- The phase transition (amorphous to cubic phase) temperature of the obtained YSZ precursor powders is as low as around 400 °C in the case of ammonium hydroxide co-precipitation method, while it is around 500 °C when ammonium bicarbonate, oxalic acid, and urea are used as precipitants.
- Ammonium bicarbonate cannot precipitate ZrO^{2+} effectively in the solution, resulting in the formation of cubic $Y_{0.18}Zr_{0.82}O_{1.91}$ at 1000 °C.
- Despite the time-consuming co-precipitation process, urea was proved to be the optimal precipitant to prepare YSZ nanocrystalline powders with designed Y/Zr/O molar ratio, large surface area, small crystallite size, and well dispersion.

Keywords: YSZ · Nanocrystalline powders · Co-precipitation · Precipitant

1 Introduction

Based on its high thermal expansion coefficient, low thermal conductivity, high ionic conductivity, and desirable thermal and chemical stability [1], yttrium-stabilized zirconia ($Y_{0.08}Zr_{0.92}O_{1.96}$, YSZ) finds wide applications in high-temperature structural materials [2, 3], thermal barrier coatings [4, 5], catalysis [6], and electrolyte for solid oxide fuel cells [7, 8]. In all these applications, crystallite/grain size plays an important role in property modification of materials. Compared to bulk materials, nanostructured materials have a wide functional diversity and exhibit enhanced or different properties. For example, nanocrystalline rare-earth-stabilized zirconia exhibited improved radiation resistance, decreased thermal conductivity, and increased ionic conductivity as compared to its traditional microcrystalline product [9]. Besides, it is also beneficial to control the micro-morphology of nanocrystalline powders. For instance, particular consolidation and compaction properties were exhibited in ceramics sintered by agglomerate-free nanocrystalline powders with narrow size distribution [10]. Thus, synthesis of YSZ high-quality nanocrystalline powders with well dispersion is of great importance for obtaining these desirable properties.

In order to obtain highly dispersed YSZ nanoparticles, several methods have been explored, including co-precipitation [11, 12], spray freeze drying [13], sol–gel route [14], and hydrothermal method, and so on [15]. Most of these build-up processes unfortunately have several inherent disadvantages associated with their production cost, complexity, and speed of operation [11]. Among these methods, co-precipitation method turns out to be a promising selection owning to its advantages on simplicity, ecological compatibility, possibility to control microstructure, and prospect on large-scale production [16, 17]. However, nanocrystalline powders prepared by the co-precipitation method exhibit different characteristics in particle shape, size, and dispersity, which are highly influenced by precipitants [18–21]. So, the selection of precipitant is very important in co-precipitation preparation. Typically, precipitants used in the co-precipitation route are ammonium hydroxide (AH), ammonium bicarbonate (AB) (or ammonium carbonate), urea, oxalic acid, and others. However, existing literatures contain few studies on YSZ nanocrystalline powders synthesized by co-precipitation method with various types of precipitants. Thus, it is necessary to investigate the effects of precipitants on the characteristics of YSZ nanocrystalline powders. In this study, YSZ nanocrystalline powders were prepared by co-precipitation method in which four different widely used precipitants, including ammonia hydroxide, AB, oxalic acid, and urea, which can provide different pH ranges in the solution, were employed to investigate their effects on phase evolutions, micro-morphologies, and surface areas of as-obtained nanocrystalline powders.

2 Experimental details

$ZrOCl_2{\cdot}8H_2O$ and $Y(NO_3)_3{\cdot}6H_2O$ were used as starting materials and dissolved in deionized water to form a 125-ml mother solution ($C_{Zr} = 0.2$ mol/l) in which ZrO^{2+} and Y^{3+} concentration meets the formula $Y_{0.08}Zr_{0.92}O_{1.96}$. Then, AH (~13 ml, 25–28wt% in water), AB (20g, analytical pure), and oxalic acid (4g, analytical pure) were added into ethanol–water solution (200 ml ethanol+800 ml water) to form three kinds of precipitation solutions, respectively. After that, the mother solution was added dropwise into these three kinds of precipitation solutions, respectively, under vigorous stirring at room temperature (25 °C). During the precipitation process, white precipitates gradually formed. The precipitates were stirred for 60min to ensure the completion of the hydrolysis reaction. When urea was used as precipitant, about 29.2g was dissolved into an ethanol–water solution (50 ml ethanol+200 ml water), and then the total mixed solution was added directly into the mother solution. The mixture was then placed in a constant temperature magnetic stirrer and stirred at 90 °C. With the increase of temperature, urea was decomposed and precipitates were gradually formed. When the pH of the solution reached to ~7.1, the stirring was stopped. After the co-precipitation process, these four types of precipitates were

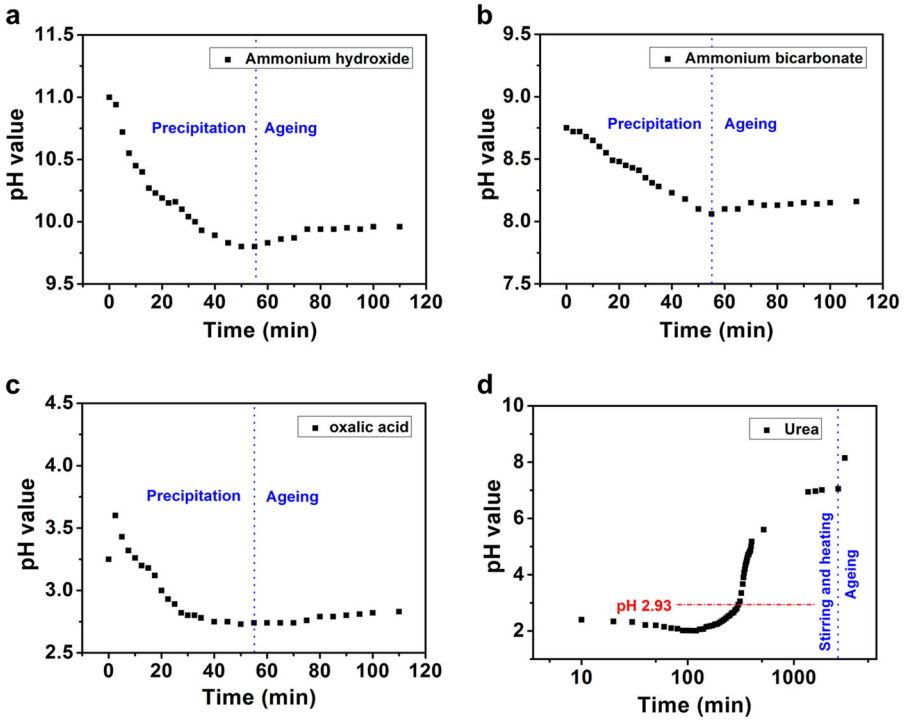

Fig. 1 pH values of the solutions as a function of time when **a** ammonium hydroxide (AH), **b** ammonium bicarbonate (AB), (**c**) oxalic acid, and (**d**) urea were used as precipitants, respectively. One hundred and twenty five milliliters of (Zr, Y) mother solution ($C_{Zr} = 0.2$ mol/l) was added drop by drop at a rate of ~2.3 ml/min into AH, AB, and oxalic acid, respectively

aging for about 6 h. Subsequently, all precipitates were centrifugally separated from the solution and washed by deionized water and then by ethanol for several times. Then, these precipitates were dried at 60 °C to get white precursor powders. Finally, the precursors were heat treated at different temperatures (300, 400, 500, and 600 °C) for 2 h in a furnace.

Thermal behavior of these four kinds of precursor powders were tested between room temperature to 1000 °C using thermogravimetric analysis (TG) and differential scanning calorimetry (DSC) analysis by NETZSCH-STA-449F3. The chemical groups of the dried precursors were detected by Fourier-transform infrared (FT-IR) analysis (Nicolet 6700) in the wavenumber range of 400–4000 cm^{-1} with the resolution of ~4 cm^{-1}. X-ray powder diffraction (XRD) patterns of YSZ powders heat treated at different temperatures were recorded on an X-ray diffractometer (DX-2700, Dandong Fangyuan, Dandong, Liaoning, China) with Cu Kα radiation ($\lambda = 1.5406$ Å) at a step size of 0.03° over a 2θ scan range of 10–70°. Scanning electron microscope (SEM, FEI, Inspect-F50) was used to investigate the micro-morphology of the 600 °C calcined powders. Specific surface areas and adsorption–desorption isotherms of YSZ powders were measured by a multipoint Brunauer–Emmett–Teller (BET) method (Tristar 3000, Micromeritics, Atlanta, GA, USA) using N_2 as the adsorbate gas.

3 Results and discussion

The pH vs. time curves were plotted and shown in Fig. 1 to reveal the pH value evolutions during co-precipitation process with AH, AB, oxalate, and urea as precipitants. During the precipitation process, the pH value of AH-precipitated process decreased from the initial 11.0 to 9.8 with a maximum variation value of 1.2. When AB was used as a precipitant, the pH value decreased slowly from 8.7 to 8.1 and the change amount of pH value was 0.6. For the oxalic acid co-precipitated process, the pH value evolves from 3.2 to 2.7 with a variation of 0.5. However, when urea was used as a precipitant, the precipitate was observed when the pH value increased slowly to ~2.9 from 2.7, and the pH value rose to ~7.1 before the aging process was started. The variation (V_x) ranking of pH value of the solutions in which different types of precipitants were used is $V_{urea} > V_{AH} > V_{AB} > V_{oxalic}$. The different pH variations were due to the different chemical reactions during the co-precipitation processes:

$$NH_4OH \leftrightarrow NH4^+ + OH^-. \quad (1)$$

$$NH_4HCO_3 + H_2O \leftrightarrow NH_4OH + H_2CO_3; NH_4OH \leftrightarrow NH_4^+ + OH^-. \quad (2)$$

$$C_2O_4H_2 \leftrightarrow C_2O_4H^- + H^+; C_2O_4H^- \leftrightarrow C_2O_4^{2-} + H^+. \quad (3)$$

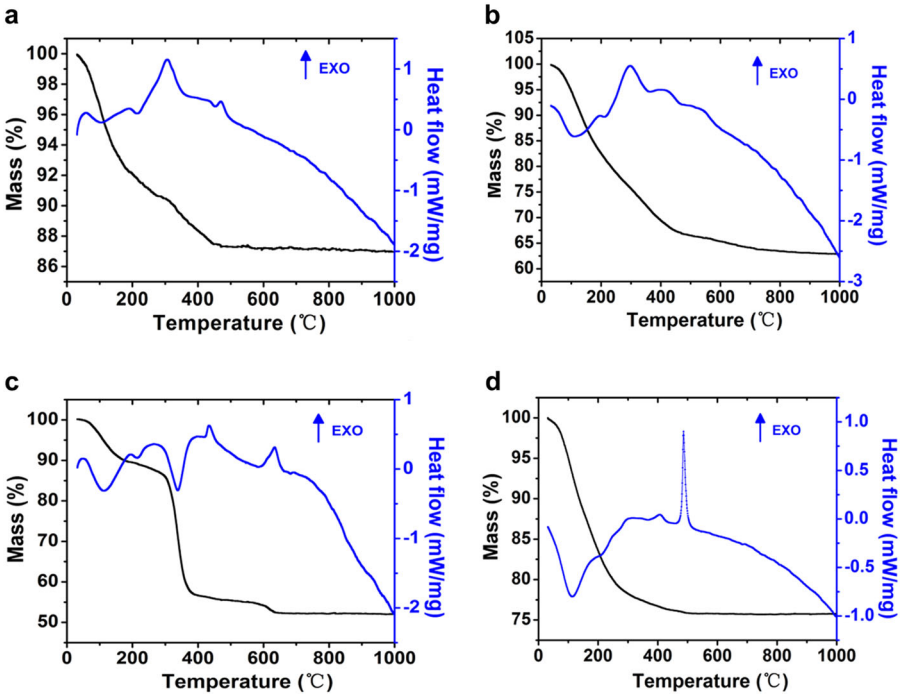

Fig. 2 Thermogravimetric analysis-differential scanning calorimetry (TG-DSC) curves of yttrium-stabilized zirconia (YSZ) dried precipitates when **a** ammonium hydroxide (AH), **b** ammonium bicarbonate (AB), **c** oxalic acid, and **d** urea are used as precipitants

$$CO(NH_2)_2 + 3H_2O \leftrightarrow CO_2 + 2NH_4OH; NH_4OH \leftrightarrow NH_4^+ + OH^- \quad (4)$$

With different precipitants, Y^{3+} (taking Y^{3+} as an example) may precipitate as $Y_2(OH)_5NO_3{\cdot}nH_2O$ ($n = 1$–3) in AH and urea method [22]. On the other hand, Y^{3+} may most likely be precipitated as normal carbonate of $[Y_2(CO_3)_3{\cdot}nH_2O$ ($n = 2$–3)] [23] or basic carbonate of $[Y(OH)CO_3]$ [24] in AB method, and as $YC_3H_6{\cdot}nH_2O$ in oxalic method [25].

Thermogravimetric analysis-differential scanning calorimetry (TG-DSC) traces of the dried precipitates prepared, respectively, with AH, AB, oxalic, and urea are given in Fig. 2. When AH and urea are served as precipitants, both ZrO^{2+} and Y^{3+} are mainly precipitated by OH^-. So these dried precipitates have similar thermal behavior. Their TG curves both show two weight losses. The first stage is associated with the removal of molecular water, and residual nitrate and ammonium ions (20–220 °C), with weight loss of 8% and 20% for AH and urea-precipitated products, respectively. The less weight loss of the dried precipitate prepared with AH may be caused by its (Zr, Y) hydroxide as it has a higher degree of dehydration. The second weight loss of about 4% observed in both of these dried precipitates may be attributed to the decomposition of zirconium hydroxide. The exothermic peaks at 470 and 490 °C in the DSC curves of the dried precipitates prepared with AH and urea, respectively, indicate the formation of nanocrystalline YSZ [26]. When AB was used as a precipitant, the weight loss of the dried precipitate at lower temperatures (<450 °C in this study) was mainly due to the release of ammonium, and dehydration and partial decomposition of the CO_3 group [27], while that which happened at higher temperatures (>450 °C in this study) was mainly caused by the further decomposition of carbonate species [28]. In the DSC curve, the broad exothermic peak at about 550 °C indicates the formation of crystalline phase. When oxalic acid was used as precipitants, the weight loss of ~15 % in temperature interval 20–220 °C is caused by the removal of adsorbed and hydrated water, evidenced by the endothermic peak in DSC curve. The second-stage weight loss in temperature interval 250–380 °C is mainly attributed to the decomposition of zirconyl oxalate ($ZrOC_2O_4$) and $Y_2(C_2O_4)_3$ [29, 30], which is an endothermic reaction. The exothermic peak at around 650 °C in DSC curve is owing to amorphous-crystalline phase transition.

In order to investigate the thermal-decomposition behavior, FT-IR measurements were employed on the dried precipitates and their calcined products at various temperatures (Fig. 3). The infrared (IR) curves shown in Fig. 3a, d confirmed that the dried precipitates prepared with AH and urea and their calcined products at 300 and 600 °C have almost the same chemical composition. However, the dried precipitates synthesized using AB and oxalic acid were different and more complex in chemical compositions compared with that prepared with AH and urea. For examples, the band at 650 cm^{-1} in Fig. 3b should be associated with the Zr-O stretching in the Zr-O-H chain [31]. And when oxalic acid was used, the peak at 895 cm^{-1} in Fig. 3c could be attributed to the C-O stretching in the

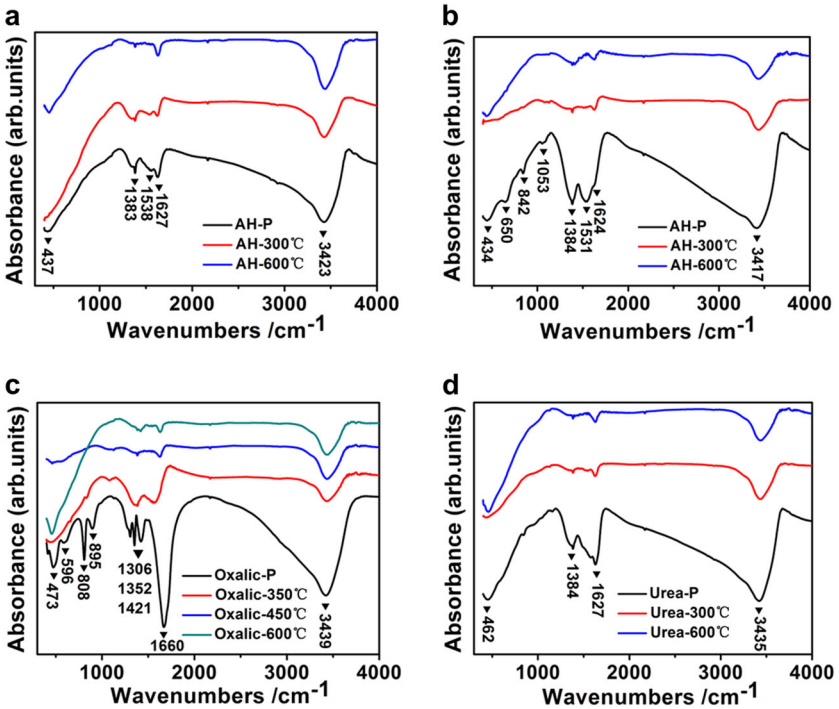

Fig. 3 Fourier-transform infrared (FT-IR) spectrums of the dried precipitates and its calcined products at various temperatures: **a** ammonium hydroxide (AH), **b** ammonium bicarbonate (AB), **c** oxalic acid, and **d** urea

Zr-O-C chain [32]. When these dried precipitates were calcined at 600 °C, all the IR curves of calcined products show similar absorption bands. The broaden absorption band at around 3430 cm^{-1} is attributed to the stretching and bending vibration of water [33]. And two bands related to carboxylate stretching modes are observed at around 1627 and 1384 cm^{-1} [29]. However, the TG curves in Fig. 2 have shown that the thermal decompositions of these four types of dried precipitates were nearly complete. So, the water and carboxylate may be derived from the absorptions from air because of high surface areas of the calcined powders.

Usually nanopowders with high specific surface areas are beneficial to sinter nanograin ceramic owing to high surface energies. Therefore, we studied the effects of precipitants on the surface area and pore size distribution of YSZ nanocrystalline powders. The N_2 absorption–desorption isotherms and surface area summary data of the samples prepared by the four different co-precipitation methods are shown in Fig. 4 and Table 1, respectively. The inner chart in Fig. 4b is an (c) enlarged view of the isotherms of oxalic acid precipitated products. Firstly, it can be found in Fig. 4a that the absorbed quantity as a function of P/P_0 of the dried precipitates is ranking as AH>urea>AB>oxalic. Interestingly, Fig. 2 shows that the total weight loss of the dried precipitates at high temperature (1000 °C) is ranking as AH<urea<AB<oxalic. Thus, adsorbent or combinative compositions may be detrimental to the adsorption properties or the specific surface areas of the dried precipitates. From Fig. 4b, we observed that the adsorption–desorption curves of the calcined powders using AH, AB, and urea methods belong to type III isotherms, while the curve of products prepared by oxalic acid co-precipitation method shows the H_3-type owing to the interconnect of agglomerated particles and the pores of interparticles creation [34]. The surface areas of the calcined powders and pores were calculated by the BET and Barrett–Joyner–Halenda (BJH) method, respectively. The surface areas of the calcined powders for the samples obtained with the AH, AB, oxalic acid, and urea co-precipitation methods were 72.25, 78.02, 24.14, and 84.19 m^2/g, respectively. The adsorption and desorption surface area of pores between 1.7 and 300 nm for samples obtained with the AH, AB, oxalic acid, and urea co-precipitation methods were 69.15, 84.46, 27.06, and 91.08g and 92.97, 110.26, 31.05, and 119.08 m^2/g, respectively. According to the BET and BJH data, the powder synthesized by urea co-precipitation method shows the highest dispersity and the largest surface area of pores. In contrast to other synthesized zirconia powders at the same calcination temperature, which have the BET surface area between 35 and 145 m^2/g [35], the synthesized powder prepared with urea in this work still shows fine BET performance.

To investigate the phase evolutions of the precursor powders prepared with four different precipitants, X-ray diffraction patterns of powders calcined at 300, 400, 500, and 600 °C were recorded and shown in Fig. 5. At 400 °C, only the powders prepared with AH shows a crystalline phase (Fig. 5a) and the remaining samples synthesized using other precipitants were amorphous (Fig. 5b–d). Up to 500 °C, four kinds of calcined powders are crystallined and

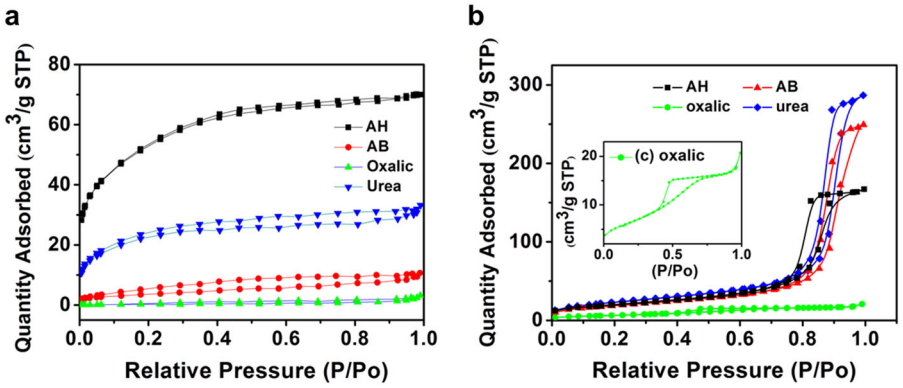

Fig. 4 N_2 adsorption–desorption isotherms for **a** the dried precipitates and **b** their calcined products at 600 °C prepared with **a** ammonium hydroxide (AH), **b** ammonium bicarbonate (AB), **c** oxalic acid, and **d** urea

Table 1 BET surface area and BJH adsorption–desorption surface area of pores between 1.7and 300 nm data for the calcined products at 600 °C

Samples	AH	AB	Oxalic	Urea
BET surface area (m^2/g)	72.25 ± 0.20	78.02 ± 0.33	24.14 ± 0.16	84.19 ± 0.30
BJH adsorption surface area of pores (m^2/g)	69.45 ± 0.30	84.46 ± 0.26	27.06 ± 0.11	91.08 ± 0.29
BJH desorption surface area of pores (m^2/g)	92.97 ± 0.22	110.26 ± 0.17	31.05 ± 0.20	119.08 ± 0.33

BET Brunauer–Emmett–Teller, *BJH* Barrett–Joyner–Halenda, *AH* ammonium hydroxide, *AB* ammonium hydroxide

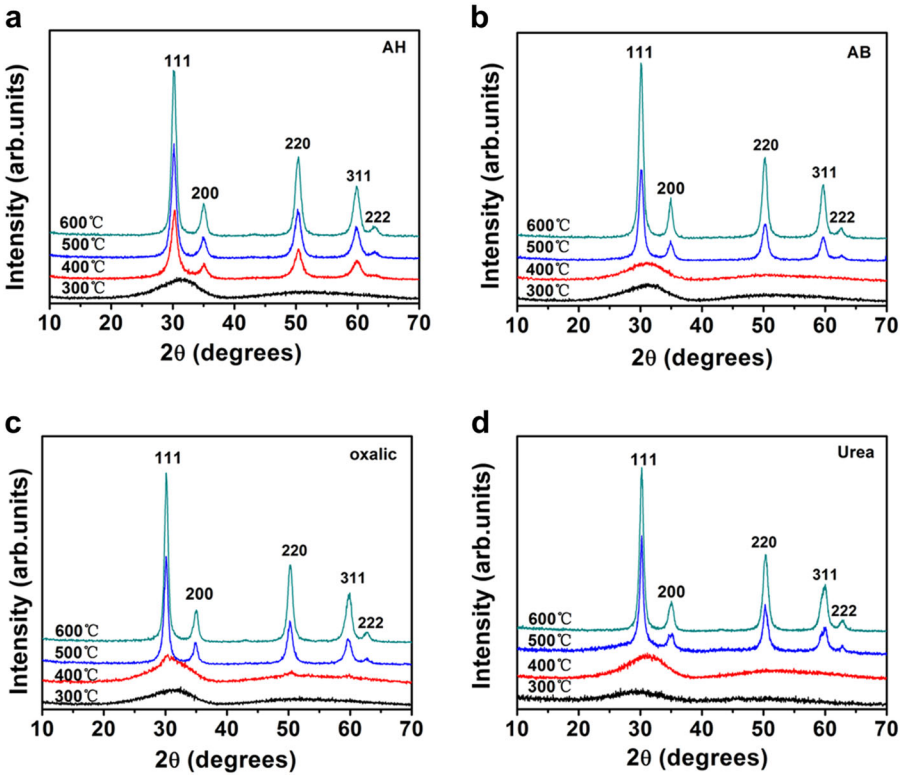

Fig. 5 X-ray powder diffraction (XRD) patterns for the calcined products of dried precipitates obtained with four different types of precipitants at 300, 400, 500, and 600 °C: **a** ammonium hydroxide (AH), **b** ammonium bicarbonate (AB), **c** oxalic acid, and **d** urea

showed the cubic structure. It can be concluded that the crystallization temperature of AH method is below 400 °C, while others were between 400 and 500 °C. The crystallization temperature derived from TG-DSC curves in Fig. 2 is about 470, 550, 650, and 490 °C, higher than that derived from the XRD results. These differences may be attributed to that the powders for XRD test were calcined for 2 h. With the increase of temperature to 600 °C, more sharpened peaks can be observed and no phase transition occurs. Since zirconia is a polymorphic (monoclinic, tetragonal, or cubic) material, the thermal-driven phase evolutions were further investigated. Figure 6 shows the XRD patterns of four types

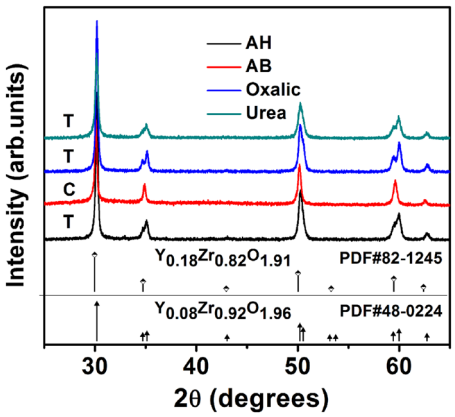

Fig. 6 X-ray powder diffraction (XRD) patterns of four types of calcined products at 1000 °C. $Y_{0.18}Zr_{0.82}O_{1.91}$ (PDF#82-1245) is a cubic phase (C) and $Y_{0.08}Zr_{0.92}O_{1.96}$ (PDF#48-0224) is a tetragonal phase (T)

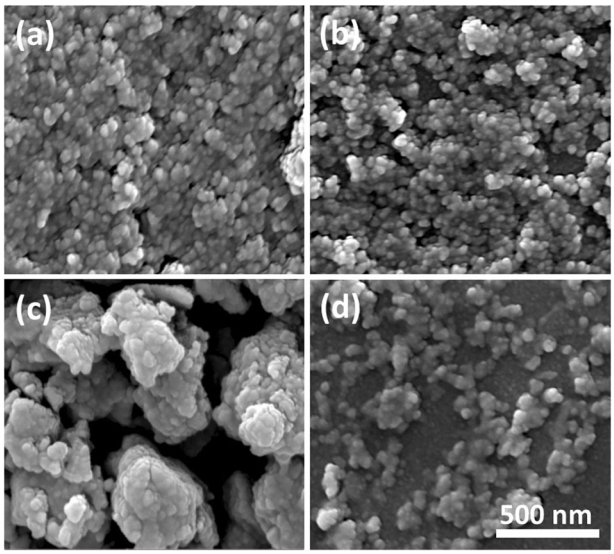

Fig. 7 Scanning electron microscope (SEM) images for the calcined products of dried precipitates obtained with four different types of precipitants at 600 °C: **a** ammonium hydroxide (AH), **b** ammonium bicarbonate (AB), **c** oxalic acid, and **d** urea

of calcined products at 1000 °C. It can be found that the crystal structures of calcined products prepared with AH, oxalic acid, and urea transformed to the tetragonal phase from the cubic phase. Diffraction peaks of these calcined products corresponded well with that of $Y_{0.08}Zr_{0.92}O_{1.96}$ (PDF#48-0224). The tetragonal ZrO_2 is a desirable phase for it avoids the volume expansion of traditional low-temperature monoclinic phase transferring to intermediate-temperature tetragonal phase, resulting in a good long-term durability with high strain compliance and the long-term thermal stability at high temperature [36, 37]. However, the calcined product prepared with AB still shows a cubic structure, evidenced by the diffraction peaks that are identical with that of $Y_{0.18}Zr_{0.82}O_{1.91}$ (PDF#82-1245). These results suggest the element loss of Zr during the fabrication process when AB was served as precipitant. This issue will be further verified in the later paragraphs.

In order to check the influence of the different precipitants (AH, AB, oxalic, and urea) on micro-morphology properties of the synthesized powders and whether Y ions were successful doped, SEM were employed. Figure 7 shows the SEM images of powders calcined at 600 °C using the four different co-precipitation methods. As shown in the Fig. 7, the dispersion differences can be clearly seen. Using AH as precipitant results in agglomerated nanoparticles in irregular shape with average particle size of around 40 ± 8 nm (Fig. 7a). However, particle shape of the powders produced by AB method seems to be more homogeneous. This was likely attributed from the homogenous co-precipitation process, which provides the formation of the spherical-like particles. The average size of primary particle is around 35 ± 5 nm (Fig. 7b). Compared with the AH method, the nanoparticles prepared by the AB method showed more uniform and spherical shape and less aggregation. However, the particles prepared in such a way are also agglomerated.

When oxalic acid was used as a precipitant, the obtained powders exhibit the worst dispersity. The secondary particles with an average size of around 500 ± 140 nm consisted of irregular aggregated primary particles (Fig. 7c). This may be attributed to the close-range YSZ crystal nucleus merged and grew up during the calcination process. Among them, nanoparticles owning the highest dispersity and the least agglomeration were observed in the case of urea-based co-homogeneous precipitation. From Fig. 7d, the morphology of nanoparticles was found to be highly dispersed, with an average primary particle size of around 35 ± 6 nm. During the co-precipitation process, urea served as a reservoir of precipitating anions. In situ decomposition of urea releases precipitating ligands (OH^- and CO_3^{2-}) slowly and homogeneously into the reaction system above 90 °C; thus, slowing and controlling the reaction rate avoid localized distribution. Considering that the mono-dispersed nanoparticle was desired characteristics, the priority of methods for obtaining desired nanoparticles is ranking as urea>AB>AH>oxalic. This ranking is agreed well with the BET surface areas of the calcined powders at 600 °C. The result that urea facilitates to fabricate nanocrystalline powders with fine microstructure is consistent well with that in other nanoparticles [38–40]. Moreover, with the same co-precipitation method, our synthesized YSZ nano-powder shows better particle characteristics in terms of particle size, shape, and dispersity than that in refs [41, 42].

In Fig. 6, we considered that the atomic ratio of Zr in the nanocrystalline powders prepared with AB may be less than the theoretical value. Thus, energy-dispersive spectrometer

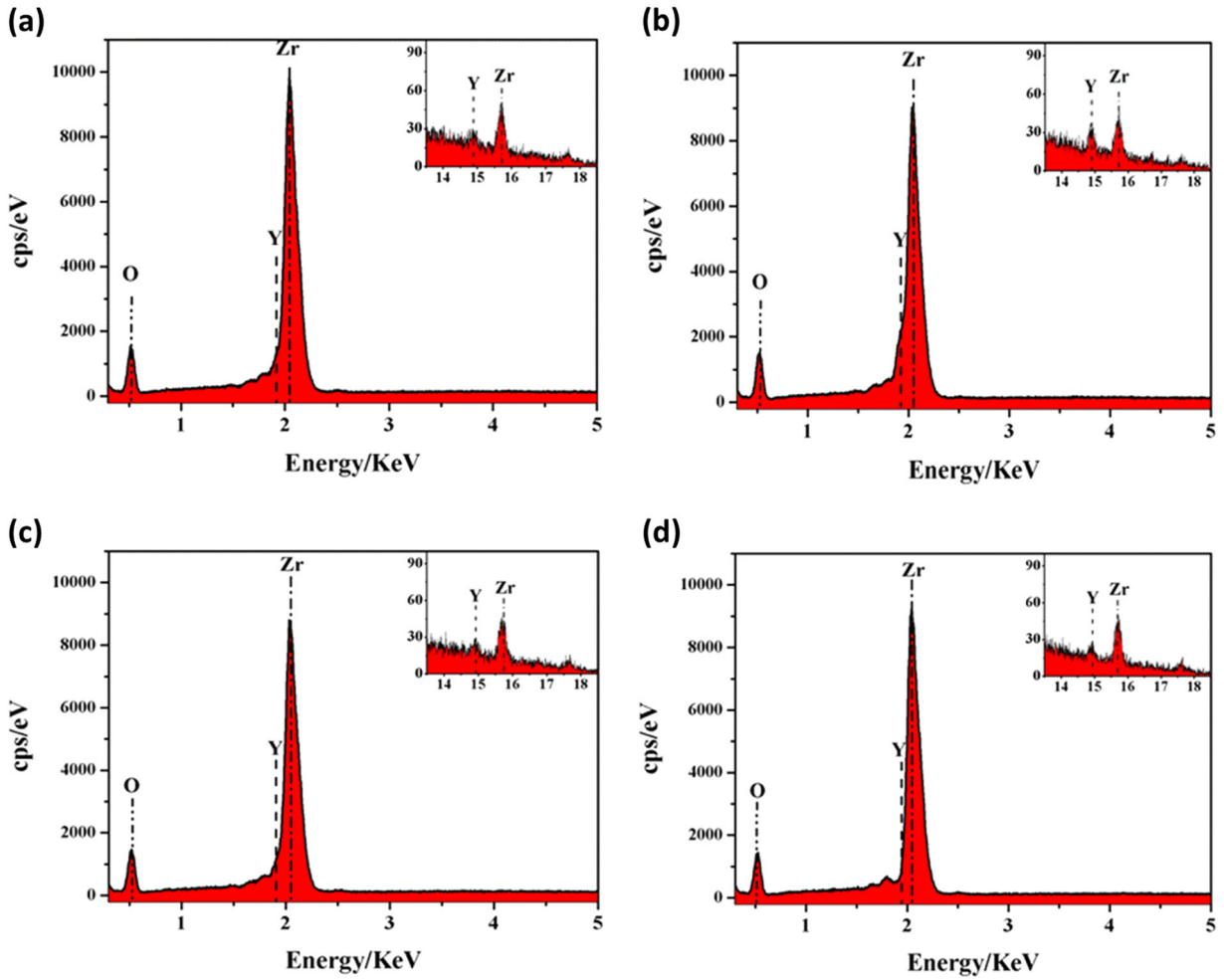

Fig. 8 Energy-dispersive spectrometer (EDS) analysis curves for the calcined products of dried precipitates obtained with four different types of precipitants at 600 °C: **a** ammonium hydroxide (AH,) (**b**) ammonium bicarbonate (AB), **c** oxalic acid, and **d** urea

(EDS) and X-ray photoelectron spectroscopy (XPS) were employed to verify this result. Figure 8 shows the EDS analysis curves for the powders obtained with the AH, AB, oxalic acid, and urea co-precipitation methods, respectively. The spectrum peaks indicate that Y was successfully doped in ZrO_2 for all samples. It is worth noting that the relative intensity ratio of Y/Zr spectrum peaks in samples prepared by the AB method was the largest, indicating a higher Y atomic percent in the prepared powders. The chemical formulas derived on the basis of EDS results are listed in Table 2. It shows that the calcined powders prepared with AB have a chemical formula of $Y_{0.18}Zr_{0.82}O_{1.91}$, corresponding well with XRD results presented in Fig. 6. The XPS lineshapes of Zr_{3d} and Y_{3d} spectra are displayed in Fig. 9 and the atomic ratios of Y and Zr calculated by XPS are also displayed in Table 2. Since the designed chemical formula is $Y_{0.08}Zr_{0.92}O_{1.96}$, the XPS result confirms that the atomic ratio of Zr in the nanocrystalline powders prepared with AB may be less than the theoretical value. However, the tested chemical formulas (XRD, EDS, and XPS results) of nanocrystalline powders prepared with AH, oxalic, and urea are close to the designed one, suggesting that AH, oxalic acid, and urea were appropriate precipitants to co-precipitate Y^{3+} and ZrO^{2+} in the solution with designed molar ratio.

Table 2 Summary of EDS-derived atomic percent of Y and Zr, and calculated chemical formulas using EDS and XPS analysis

	EDS		XPS	
	Y (at%)	Zr (at%)	Chemical formula	Chemical formula
AH	2.78	25.26	$Y_{0.10}Zr_{0.90}O_{1.95}$	$Y_{0.13}Zr_{0.87}O_{1.94}$
AB	5.05	22.85	$Y_{0.18}Zr_{0.82}O_{1.91}$	$Y_{0.21}Zr_{0.79}O_{1.90}$
Oxalic	2.89	23.79	$Y_{0.11}Zr_{0.89}O_{1.95}$	$Y_{0.12}Zr_{0.88}O_{1.94}$
Urea	1.97	25.89	$Y_{0.07}Zr_{0.93}O_{1.97}$	$Y_{0.12}Zr_{0.88}O_{1.94}$

EDS energy-dispersive spectrometer, *XPS* X-ray photoelectron spectroscopy, *AH* ammonium hydroxide, *AB* ammonium bicarbonate

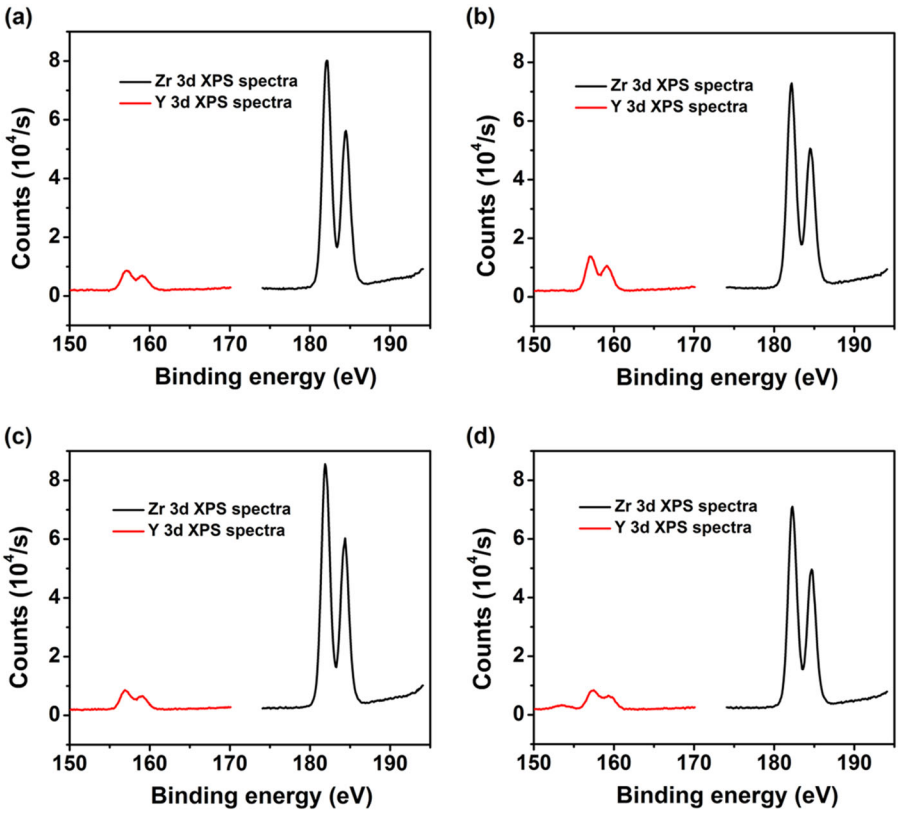

Fig. 9 X-ray photoelectron spectroscopy (XPS) analysis of the calcined products of dried precipitates obtained with four different types of precipitants at 1000 °C: **a** ammonium hydroxide (AH), **b** AB, **c** oxalic acid, and **d** urea

4 Conclusion

The effects of precipitants on co-precipitation synthesis of $Y_{0.08}Zr_{0.92}O_{1.96}$ nanocrystalline powders were investigated in this work. Using AH, AB, oxalic acid, and urea as precipitants, the precursor powders are fully decomposed at around 600 °C. The phase transition (amorphous to cubic phase) temperature of the precursor powders is as low as around 400 °C in the case of AH co-precipitation method, while is around 500 °C when AB, oxalic acid, and urea are used as precipitants. Tetragonal phase was observed as the powder calcination temperature increased to 1000 °C when AH, oxalic, and urea are used as precipitants, while cubic $Y_{0.18}Zr_{0.82}O_{1.91}$ was obtained in the case of AB co-precipitation method. AB was proved not to be an appropriate precipitant to be able to co-precipitate Y^{3+} and ZrO^{2+} with designed molar ratio in the solution. Despite the time-consuming co-precipitation process, urea was proved to be the optimal precipitant to prepare YSZ nanocrystalline powders with designed Y/Zr/O molar ratio, large surface area, small crystallite size, and well dispersion.

Acknowledgements This work was supported by the National Natural Science Foundation of the People's Republic of China under Grant Nos. 11505122 and 11775152, the Science and Technology Innovation Team of Sichuan province under Grant No.15CXTD0025, and the Key Applied Basic Research (2017JY0329) of Sichuan province.

Compliance with ethical standards

Conflict of interest The authors declare that they have no conflict of interest.

Publisher's note: Springer Nature remains neutral with regard to jurisdictional claims in published maps and institutional affiliations.

References

1. Wu Y, Bandyopadhyay A, Bose S (2004) Processing of alumina and zirconia nano-powders and compacts. Mater Sci Eng A 380 (1–2):349–355
2. Mebrahitom Asmelash G, Mamat O, Ahmad F, Prasada Rao AK (2015) Thermal shock and fatigue behavior of pressureless sintered Al_2O_3–SiO_2–ZrO_2 composites. J Adv Ceram 4(3):190–198
3. Blaese D, Garcia DE, Guglielmi P, Hotza D, Fredel MC, Janssen R (2015) ZrO_2 fiber-matrix interfaces in alumina fiber-reinforced model composites. J Eur Ceram Soc 35(5):1593–1598
4. Wang L, Shao F, Zhong XH, Ni JX, Yang K, Tao SY, Wang Y (2018) Tailoring of self-healing thermal barrier coatings via finite element method. Appl Surf Sci 431:60–74
5. Wang J, Sun J, Zhang H, Dong S, Jiang J, Deng L, Zhou X, Cao X (2018) Effect of spraying power on microstructure and property of nanostructured YSZ thermal barrier coatings. J Alloy Compd 730:471–482
6. Białas A, Kondratowicz T, Drozdek M, Kuśtrowski P (2015) Catalytic combustion of toluene over copper oxide deposited on two types of yttria-stabilized zirconia. Catal Today 257:144–149

7. Liu C, Zhang H, Xia J, Li Z (2013) Synthesis and characterization of $Zr_{0.85}Y_{0.15}O_{1.925}$-$La_{9.33}Si_6O_{26}$ composite electrolyte for application in SOFCs. J Adv Ceram 1(4):327–335
8. Carneiro JSA, Brocca RA, Lucena MLRS, Nikolla E (2017) Optimizing cathode materials for intermediate-temperature solid oxide fuel cells (SOFCs): Oxygen reduction on nanostructured lanthanum nickelate oxides. Appl Catal B 200:106–113
9. Huang Z, Qi J, Zhou M, Gong Y, Shi Q, Yang M, Han W, Cao Z, Peng S, Lu T (2018) A facile solvothermal method for high-quality $Gd_2Zr_2O_7$ nanopowder preparation. Ceram Int 44 (2):1334–1342
10. Arora A (2004) Ceramics in nanotech revolution. Adv Eng Mater 6(4):244–247
11. Xi X, Abe H, Naito M (2014) Effect of composition on microstructure and polarization resistance of solid oxide fuel cell anode Ni-YSZ composites made by co-precipitation. Ceram Int 40 (10):16549–16555
12. Aruna ST, Balaji N, Shri Prakash B (2011) Low temperature assisted chemical coprecipitation synthesis of 8YSZ plasma sprayable powder for solid oxide fuel cells. Int J Hydrogen Energy 36(22):14963–14970
13. Zhang Y, Binner J, Rielly C, Vaidhyanathan B (2014) Comparison of spray freeze dried nanozirconia granules using ultrasonication and twin-fluid atomisation. J Eur Ceram Soc 34 (4):1001–1008
14. Taherian M, Rojaee R, Fathi M, Tamizifar M (2014) Effect of different sol-gel synthesis processes on microstructural and morphological characteristics of hydroxyapatite-bioactive glass composite nanopowders. J Adv Ceram 3(3):207–214
15. Zhang F, Batuk M, Hadermann J, Manfredi G, Mariën A, Vanmeensel K, Inokoshi M, Van Meerbeek B, Naert I, Vleugels J (2016) Effect of cation dopant radius on the hydrothermal stability of tetragonal zirconia: grain boundary segregation and oxygen vacancy annihilation. Acta Mater 106:48–58
16. Zeng M, Ma Y, Wang Y, Pei C (2012) The effect of precipitant on co-precipitation synthesis of yttrium aluminum garnet powders. Ceram Int 38(8):6951–6956
17. Hsu YW, Yang KH, Chang KM, Yeh SW, Wang MC (2011) Synthesis and crystallization behavior of 3mol% yttria stabilized tetragonal zirconia polycrystals (3Y-TZP) nanosized powders prepared using a simple co-precipitation process. J Alloy Compd 509(24):6864–6870
18. Han X, Liang Z, Feng L, Wang W, Chen J, Xue C, Zhao H (2015) Co-precipitated synthesis of Al_2O_3–ZrO_2 composite ceramic nanopowders by precipitant and drying method regulation: a systematic study. Ceram Int 41(1):505–513
19. Wang Z, Zhang W, You B, Yin M (2008) Effects of precipitant on microstructure and luminescent properties of Lu_2O_3:Eu^{3+} nanopowders and ceramics. Spectrochim Acta Part A 70(4):835–839
20. Ke S, Wang Y, Pan Z (2015) Effects of precipitant and surfactant on co-precipitation synthesis of $Nd_2Si_2O_7$ ceramic pigment. Dyes Pigments 118:145–151
21. Zhang K, Liu HZ, Wu YT, Hu WB (2008) Co-precipitation synthesis and luminescence behavior of Ce-doped yttrium aluminum garnet (YAG:Ce) phosphor: the effect of precipitant. J Alloy Compd 453(1–2):265–270
22. Holcombe CE (1978) Yttria hydroxy-salt binders. J Am Ceram Soc 61(11-1):481–486
23. Saito N, Matsuda S, Ikegami T (1998) Fabrication of transparent yttria ceramics at low temperature using carbonate-derived powder. J Am Ceram Soc 81(8):2023–2028
24. Sordelet D, Akinc M (1988) Preparation of sphercal, monosized Y_2O_3 precursor particles. J Colloid Interf Sci 122(1):47–59
25. Patil DS, Prabhakaran K, Durgaprasad C, Gokhale NM, Samui AB, Sharma SC (2009) Synthesis of nanocrystalline 8 mol% yttria stabilized zirconia by the oleate complex route. Ceram Int 35 (1):515–519
26. Mahendran R, Kumaresh Babu SP, Natarajan S, Manivannan S, Vallimanalan A (2017) Phase transformation and crystal growth behavior of 8mol% ($SmO_{1.5}$, $GdO_{1.5}$, and $YO_{1.5}$) stabilized ZrO_2 powders. Int J Min Mater 24(7):842–849
27. Hayashi K, Toyoda S, Takebe H, Morinaga K (1991) Phase-transformations of alumina derived from ammonium aluminum carbonate hydroxide (AACH). J Ceram Soc Jpn 99(7):550–555
28. Head EL, Holley Jr CE (1963) The preparation and thermal decomposition of the carbonates of Tb, Dy, Ho, Er, Tm, Yb, Lu, Y, and Sc. (No. LADC-6082; CONF-405-3). Los Alamos Scientific Lab., New Mexico
29. Farhikhteh S, Maghsoudipour A, Raissi B, Mozaffari B (2008) Synthesis of high specific surface area YSZ (ZrO_2–$8Y_2O_3$) nanocrystalline powder by modified polymerized complex method. J Sol-Gel Sci Technol 49(1):60–65
30. Ipek M, Zeytin S, Bindal C (2011) An evaluation of Al_2O_3–ZrO_2 composites produced by coprecipitation method. J Alloy Compd 509(2):486–489
31. Heshmatpour F, Aghakhanpour RB (2011) Synthesis and characterization of nanocrystalline zirconia powder by simple sol–gel method with glucose and fructose as organic additives. Powder Technol 205(1–3):193–200
32. Amirsardari Z, Aghdam RM, Salavati-Niasari M, Shakhesi S (2016) Facile carbothermal reduction synthesis of ZrB_2 nanoparticles: the effect of starting precursors. Mater Manuf Proc 31 (2):134–140
33. Bineesh KV, Kim DK, Cho HJ, Park DW (2010) Synthesis of metal-oxide pillared montmorillonite clay for the selective catalytic oxidation of H_2S. J Ind Eng Chem 16(4):593–597
34. Kuo CW, Lee KC, Yen FL, Shen YH, Lee HE, Wen SB, Wang MC, Stack MM (2014) Growth kinetics of tetragonal and monoclinic ZrO_2 crystallites in 3 mol% yttria partially stabilized ZrO_2 (3Y-PSZ) precursor powder. J Alloy Compd 592:288–295
35. Pandey AK, Biswas K (2014) Effect of agglomeration and calcination temperature on the mechanical properties of yttria stabilized zirconia (YSZ). Ceram Int 40(9):14111–14117
36. Mao J, Deng Z, Liu M, Deng C, Song J, Yang K (2017) Regional characteristics of YSZ coating prepared by expanded Ar/He/H plasma jet at very low pressure. Surf Coat Technol 328: 240–247
37. Zhou Y, Yuan W, Huang Q, Huang W, Cheng H, Liu H (2015) Effect of Y_2O_3 addition on the phase composition and crystal growth behavior of YSZ nanocrystals prepared via coprecipitation process. Ceram Int 41(9):10702–10709
38. Dulina NA, Yermolayeva YV, Tolmachev AV, Sergienko ZP, Vovk M, Vovk EA, Matveevskaya NA, Mateychenko PV (2010) Synthesis and characterization of the crystalline powders on the basis of Lu_2O_3: Eu^{3+} spherical submicron-sized particles. J Eur Ceram Soc 30(7):1717–1724
39. Kafili G, Movahedi B, Milani M (2016) A comparative approach to synthesis and sintering of alumina/yttria nanocomposite powders using different precipitants. Mater Chem Phys 183:136–144
40. Jung YS, Yoon WL, Seo YS, Rhee YW (2012) The effect of precipitants on Ni-Al_2O_3 catalysts prepared by a co-precipitation method for internal reforming in molten carbonate fuel cells. Catal Commun 26:103–111
41. Dong X, Li F, Zhao N, Xiao F, Wang J, Tan Y (2016) CO_2 hydrogenation to methanol over Cu/ZnO/ZrO_2 catalysts prepared by precipitation-reduction method. Appl Catal B 191:8–17
42. Zinatloo-Ajabshir S, Salavati-Niasari M (2016) Preparation of nanocrystalline cubic ZrO_2 with different shapes via a simple precipitation approach. J Mater Sci Mater Electron 27(4):3918–3928